Shape Optimization Analysis of Flow Field*
(Growth-Strain Method Approach)

Eiji KATAMINE**, Hideyuki AZEGAMI***
and Akiyoshi OKITSU**

A new analytical approach for optimizing shapes of the flow field is presented. The reshaping is accomplished by the growth-strain method which was first developed using the finite-element calculation of the deformation of shapes by generating bulk strain for solid problems. The generation law of the bulk strain is given as a function of a distributed parameter to be made uniform. For solid problems, the validity of the use of the shear strain energy density to maximize the strength based on the Mises criterion or the strain energy density to maximize the stiffness for the distributed parameter has been confirmed. In the present paper, we propose the use of the dissipation energy density for the distributed parameter to minimize the total energy dissipated due to the viscosity of the fluid. Numerical results for abruptly enlarged channel problems in steady state assuming low Reynolds number and incompressible viscous fluid shows the validity of the present approach.

Key Words: Optimum Design, Computational Fluid Dynamics, Pipe Line, Numerical Analysis, Finite-Element Method

1. Introduction

The objective of the present paper is to propose a new analytical method to optimize shapes of the viscous flow field in a steady state. The minimization of total energy dissipated due to viscosity is considered to be the criterion of optimality.

A guideline for optimization of the flow field can be obtained through the classical investigation[1] made on pipelines whose cross sections were gradually enlarged under the conditions of constant velocity and constant dissipation energy per unit length. Comparing these pipelines, the investigation revealed that the total energy loss of the pipeline with increased constant dissipation energy per unit length was less than that of the pipeline with increased constant velocity. The results of this investigation, suggest that minimization of the total dissipation energy can be carried out by making the locally defind dissipation energy uniform.

In the case of continuous flow field problems, the dissipation energy locally defined becomes the dissipation energy density defined per unit volume. Our examination in this paper focuses on whether or not the total dissipation energy in a continuous flow field can be minimized through the deformation that makes the distribution of the dissipation energy density uniform.

In our previous studies[2]-[6] on solid problems, it was confirmed that maximization of the strength based on the Mises criterion can be carried out by making the distribution of the shear strain energy density uniform, and that maximization of the stiffness, or minimization of the compliance, can be achieved by making the distribution of the strain energy density uniform. The reshaping to make these distributed parameters uniform has been carried out by the growth-strain method which had been proposed as a shape optimization method which use the finite-element calculation of the deformation of shapes by

* Received 30th September, 1992. Paper No. 91-1434
** Department of Mechanical Engineering, Gifu National College of Technology, 2236-2 Kamimakuwa, Shinsei-cho, Motosu-gun, Gifu 501-04, Japan
*** Department of Energy Engineering, Toyohashi University of Technology, 1-1 Hibarigaoka, Tempaku-cho, Toyohashi 441, Japan

generating bulk strain of swelling and contacting. The generation law of the bulk strain was given as a simple increasing function of a distributed parameter to be made uniform[2].

Based on the previous studies on solid problems, we use the growth-strain method as the shape deformation technique for making the distribution of the dissipation energy density uniform. The validity of the present approach for minimizing the total dissipation energy is discussed based on numerical results for two-dimensional abruptly enlarged channel problems.

2. Growth-Strain Method

The growth-strain method was proposed as a shape optimization method by generating bulk strain which causes a distributed parameter to be made locally uniform. Therefore, in the case of the optimum criterion that is given as a uniform condition of a distributed parameter, the growth-strain method is directly applicable. Maximization of the strength based on the Mises criterion means minimizing the maximum value of the shear strain energy density, which is identical to making the distribution of the shear strain energy density under a constant volume uniform. In this case, the growth-strain method can be applied by setting the shear strain energy density as the distributed parameter.

When we consider the maximization of a nondistributed integral parameter such as the potential energy, which has the meaning of stiffness, the applicability of the growth-strain method depends on the existence of an equivalent condition written with uniform conditions of a distributed parameter. In the case of the maximization problem of the potential energy in static elastic problems, we can show equivalency of the maximum condition of the potential energy to the uniform condition of the potential energy density in shape variation. Therefore, the growth-strain method becomes applicable to this problem when the potential energy density is set to the distributed parameter to be made uniform[5].

However, in the case of a viscous flow field in the steady state, we cannot obtain any uniform conditions which are equivalent to the minimum condition of the total dissipation energy or other total parameters integrated over the entire flow field, because we cannot show the existence of any functional Euler equations which can become Navier-Stokes and continuity equations.

Therefore, as a convenient alternative, we can consider a local minimization problem such that the dissipation energy density is minimized under constant volume at each local point. The minimization problem becomes identical to the problem of making the dissipation energy density uniform under constant volume. The dissipation energy density $D(\boldsymbol{x})$ is defined as

$$D(\boldsymbol{x})=2\mu\dot{\varepsilon}_{ij}(\boldsymbol{x})\dot{\varepsilon}_{ij}(\boldsymbol{x})+\lambda\dot{u}_{i,i}(\boldsymbol{x})\dot{u}_{i,i}(\boldsymbol{x}) \quad (\boldsymbol{x}\in\Omega), \tag{1}$$

where the strain velocity tensor $\dot{\varepsilon}_{ij}(\boldsymbol{x})$ is expressed by the velocity $\dot{u}_i(\boldsymbol{x})$as

$$\dot{\varepsilon}_{ij}(\boldsymbol{x})=\frac{1}{2}\{\dot{u}_{i,j}(\boldsymbol{x})+\dot{u}_{j,i}(\boldsymbol{x})\} \quad (\boldsymbol{x}\in\Omega). \tag{2}$$

Here, μ and λ are viscosity coefficients. In the case of incompressible viscous fluid, the second term on the right side of Eq. (1) is neglected. The Einstein summation convention and the partial differentiation notation $(\ ),_i=\partial(\ )/\partial x_i$ are used in this paper.

Implementation of the shape optimization analysis for flow fields using the growth-strain method consists of iteration of the two steps shown in Fig. 1. In the upper step, the dissipation energy density $D(\boldsymbol{x})$ is analyzed under mechanical conditions such as the Navier-Stokes and the continuity equations and boundary conditions. For this analysis, the finite-element method[7] is used in the present study. In the lower step, we analyze the shape deformation caused by generation of the following bulk strain:

$$\varepsilon^B_{ij}(\boldsymbol{x})=\frac{D(\boldsymbol{x})-\bar{D}}{\bar{D}}h\delta_{ij} \quad (\boldsymbol{x}\in\Omega), \tag{3}$$

where δ_{ij} is the Kronecker delta, and $\bar{D}$ is a constant value for normalizing $D(\boldsymbol{x})$. Except in a particular case, the volume average of $D(\boldsymbol{x})$ is substituted for $\bar{D}$. The constant value h, which has been called the growth rate, is a control parameter of the magnitude of the bulk strain at each iteration. The finite-element method is also used for this analysis.

The fundamental equations used in these steps will be shown in the third and the fourth sections.

3. Finite-Element Analysis of Flow Field

The finite-element method used for the analysis of flow fields of the upper step in Fig. 1 is based on the formulation called the Taylor-Hood formulation[8] which is one of the direct methods in which velocity

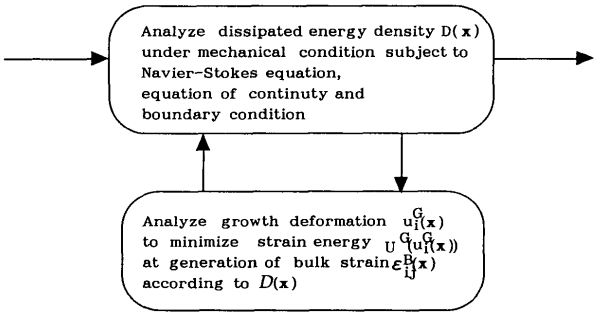

Fig. 1 Growth-strain method in flow field problems

and pressure are treated as independent variables. In this section, this formulation is clarified.

In a flow field domain Ω of a incompressible Newtonian fluid in the steady state, ignoring body forces, the Navier-Stokes and the continuity equations are given with velocity $\dot{u}_i(x)$ and pressure $p(\boldsymbol{x})$ as

$$\rho\dot{u}_j(\boldsymbol{x})\dot{u}_{i,j}(\boldsymbol{x})+p_{,i}(\boldsymbol{x})-\mu\dot{u}_{i,jj}(\boldsymbol{x})=0 \quad (\boldsymbol{x}\in\Omega) \tag{4}$$

$$\dot{u}_{i,i}(\boldsymbol{x})=0 \quad (\boldsymbol{x}\in\Omega). \tag{5}$$

On the boundary Γ of the domain Ω, considering the subindexes $i=1, 2, 3$ for $\dot{u}_i(\boldsymbol{x})(\boldsymbol{x}\in\Gamma)$ to be independent, we assume that either condition of the Dirichlet boundary condition of Eq. (6) or the Neumann boundary condition of Eq. (7) is given. Moreover, on a part of boundary Γ^p where the pressure $p(\boldsymbol{x})$ is known, we assume Eq. (8) holds:

$$\dot{u}_i(\boldsymbol{x})=\bar{\dot{u}}_i(\boldsymbol{x}) \quad (\boldsymbol{x}\in\Gamma^D=\Gamma-\Gamma^N) \tag{6}$$

$$\dot{u}_{i,j}(\boldsymbol{x})n_j(\boldsymbol{x})=\bar{\dot{u}}_{i,j}(\boldsymbol{x})n_j(\boldsymbol{x}) \quad (\boldsymbol{x}\in\Gamma^N=\Gamma-\Gamma^D) \tag{7}$$

$$p(\boldsymbol{x})=\bar{p}(\boldsymbol{x}) \quad (\boldsymbol{x}\in\Gamma^p\subset\Gamma), \tag{8}$$

where ρ is the density, and $n_i(\boldsymbol{x})$ represents the unit outer-normal vector at each point on the boundary. The notation $(\bar{\ })$ represents known quantities.

Using the standard procedure of the finite-element method, the inner velocity $\dot{u}_i(\boldsymbol{x}^e)$ within a finite element $\boldsymbol{x}^e\in\Omega^e$ is expressed, using the velocity $\dot{u}_{ai}$ at the a-th nodes and shape functions $\Phi_a(\boldsymbol{x}^e)$, as Eq. (9). The inner pressure $p(\boldsymbol{x}^e)$ is also expressed, using the pressure p_β at the β-th nodes and shape functions $\Psi_\beta(\boldsymbol{x}^e)$, which generally consist of functions with order lower than $\Phi_a(\boldsymbol{x}^e)$, as Eq. (10).

$$\dot{u}_i(\boldsymbol{x}^e)=\Phi_a(\boldsymbol{x}^e)\dot{u}_{ai} \quad (\boldsymbol{x}^e\in\Omega^e) \tag{9}$$

$$p(\boldsymbol{x}^e)=\Psi_\beta(\boldsymbol{x}^e)p_\beta \quad (\boldsymbol{x}^e\in\Omega^e) \tag{10}$$

Employing the Galerkin weighted residual approach in the domain $\Omega=\sum_e\Omega^e$, Eqs. (4) and (5) become

$$\sum_e\int_{\Omega^e}\Phi_a(\boldsymbol{x}^e)\{\rho\dot{u}_j(\boldsymbol{x}^e)\dot{u}_{i,j}(\boldsymbol{x}^e)+p_{,i}(\boldsymbol{x}^e)-\mu\dot{u}_{i,jj}(\boldsymbol{x}^e)\}dV=0 \tag{11}$$

$$\sum_e\int_{\Omega^e}\Psi_\beta(\boldsymbol{x}^e)\dot{u}_{i,i}(\boldsymbol{x}^e)dV=0. \tag{12}$$

Integration by parts of Eqs. (11) and (12) gives

$$\sum_e\int_{\Omega^e}[\Phi_a(\boldsymbol{x}^e)\{\rho\dot{u}_j(\boldsymbol{x}^e)\dot{u}_{i,j}(\boldsymbol{x}^e)+p_{,i}(\boldsymbol{x}^e)\}+\mu\Phi_{a,j}(\boldsymbol{x}^e)\dot{u}_{i,j}]dV-\sum_e\int_{\Gamma^e}\mu\Phi_a(\boldsymbol{x}^e)\dot{u}_{i,j}n_jdS=0 \tag{13}$$

$$\sum_e\int_{\Omega^e}\Psi_{\beta,i}(\boldsymbol{x}^e)\dot{u}_i(\boldsymbol{x}^e)dV-\sum_e\int_{\Gamma^e}\Psi_\beta(\boldsymbol{x}^e)\dot{u}_in_idS=0. \tag{14}$$

Substitution of Eqs. (9) and (10) for each element into Eqs. (13) and (14) gives the following governing equations:

$$M_{a\beta\gamma j}\dot{u}_{\beta j}\dot{u}_{\gamma i}+K_{ai\beta j}\dot{u}_{\beta j}+H_{ai\beta}p_\beta=\Omega_{ai} \tag{15}$$

$$H_{ai\beta}\dot{u}_{ai}=\eta_\beta, \tag{16}$$

where

$$M_{a\beta\gamma j}=\sum_e\int_{\Omega^e}\rho\Phi_a\Phi_\beta\Phi_{\gamma,j}dV \tag{17}$$

$$K_{ai\beta j}=\sum_e\int_{\Omega^e}\mu\Phi_{a,k}\Phi_{\beta,k}\delta_{ij}dV \tag{18}$$

$$H_{ai\beta}=\sum_e\int_{\Omega^e}\Phi_a\Psi_{\beta,i}dV \tag{19}$$

$$\Omega_{ai}=\sum_e\int_{\Gamma^e}\mu\Phi_a\dot{u}_{i,j}n_jdS \tag{20}$$

$$\eta_\beta=\sum_e\int_{\Gamma^e}\Psi_\beta\dot{u}_in_idS. \tag{21}$$

Substituting the boundary conditions of Eqs. (6) to (8), Eqs. (15) and (16) become nonlinear equations for the unknown variables of $\dot{u}_{ai}$ and p_β. These nonlinear equations can be solved by the Newton-Raphson method. When the value of the given velocity $\bar{\dot{u}}_i$ is large enough, to stabilize the convergence of the solution, the analyses should be performed incrementally by dividing the value into appropriate increments.

4. Shape Deformation Analysis

In this section, the finite-element method used for the shape deformation analyses of the lower step in Fig. 1 is clarified.

When the bulk strain $\varepsilon^B_{ij}(\boldsymbol{x})$ of Eq. (3) is generated over the entire domain Ω, we can define the strain energy for the deformation. Therefore, we can naturally assume that the deformation is determined from the minimum condition of the strain energy. Using the notation $x_i\in\Omega\mapsto x^G_i\equiv x_i+u^G_i\in\Omega^G$ for the shape deformation, the strain energy is given as

$$U^G(u^G(\boldsymbol{x}))=\frac{1}{2}\int_\Omega\{\varepsilon^G_{ij}(\boldsymbol{x})-\varepsilon^B_{ij}(\boldsymbol{x})\}D_{ijkl}\{\varepsilon^G_{kl}(\boldsymbol{x})-\varepsilon^B_{kl}(\boldsymbol{x})\}dV, \tag{22}$$

where the strain $\varepsilon^G_{ij}(\boldsymbol{x})$ for the shape deformation should satisfy the following compatibility condition.

$$\varepsilon^G_{ij}(\boldsymbol{x})=\frac{1}{2}\{u^G_{i,j}(\boldsymbol{x})+u^G_{j,i}(\boldsymbol{x})\} \tag{23}$$

The tensor D_{ijkl} is the elastic constitutive tensor. The minimum condition of the strain energy is obtained as

$$\delta U^G(u^G(\boldsymbol{x}))=\int_\Omega\{\varepsilon^G_{ij}(\boldsymbol{x})-\varepsilon^B_{ij}(\boldsymbol{x})\}D_{ijkl}\delta\varepsilon^G_{kl}(\boldsymbol{x})dV=0, \tag{24}$$

where δ represents the arbitrary shape deformation satisfying the shape constraints.

In the standard procedure of the finite-element method, using the matrix expression for simplicity, the inner strain vector $\{\varepsilon^G(\boldsymbol{x}^e)\}$ for the shape deformation in a finite element $\boldsymbol{x}^e\in\Omega^e$ is expressed, with the nodal displacement vector $\{\underline{u}^G\}$, as

$$\{\varepsilon^G(\boldsymbol{x}^e)\}=[B(\boldsymbol{x}^e)]\{\underline{u}^G\} \quad \{\boldsymbol{x}^e\in\Omega^e\}. \tag{25}$$

Equation (24) is rewritten, using the matrix expression in the domain $\Omega=\sum_e\Omega^e$, as

$$\sum_e \int_{\Omega^e} \delta\{\varepsilon^G(\boldsymbol{x}^e)\}^T[D]\{\varepsilon^G(\boldsymbol{x}^e)\}dV$$
$$=\sum_e \int_{\Omega^e} \delta\{\varepsilon^G(\boldsymbol{x}^e)\}^T[D]\{\varepsilon^B(\boldsymbol{x}^e)\}dV. \quad (26)$$

Substituting Eq. (25) for the whole element into Eq. (26), we can obtain the following governing equations for $\{\underline{u}^G\}$:

$$[K]\{\underline{u}^G\}=\{g\}, \quad (27)$$

where

$$[K]=\sum_e \int_{\Omega^e} [B(\boldsymbol{x}^e)]^T[D][B(\boldsymbol{x}^e)]dV \quad (28)$$

$$\{g\}=\sum_e \int_{\Omega^e} [B(\boldsymbol{x}^e)]^T[D]\{\varepsilon^B(\boldsymbol{x}^e)\}dV. \quad (29)$$

The matrix $[K]$ is the stiffness matrix and $\{g\}$ is the equivalent nodal force vector for generation of the bulk strain. The notation $(\ )^T$ represents transposition.

5. Numerical Results

Numerical examination was performed on two-dimensional abruptly enlarged channel problems.

The initial shape of the channel is shown in Fig. 2 where incompressible viscous flow is from the left side to the right side. The Reynolds number $Re=50$ was assumed. At the entrance, Poiseulle flow was assumed at the exit, the Neumman boundary condition was assumed. In fact, considering symmetry, the following boundary conditions were given:

$$\dot{u}_1(\boldsymbol{x})=\frac{3}{2}\bar{\dot{u}}\{1-\left(\frac{2}{L}\right)^2 x_2^2\}$$
and $\dot{u}_2(\boldsymbol{x})=0 \quad (\boldsymbol{x}\in[A-B])$ (30)

$$\dot{u}_1(\boldsymbol{x})=0 \text{ and } \dot{u}_2(\boldsymbol{x})=0 \quad (\boldsymbol{x}\in[B-E]) \quad (31)$$

$$\dot{u}_{1,1}(\boldsymbol{x})=0 \text{ and } \dot{u}_{2,1}(\boldsymbol{x})=0 \quad (\boldsymbol{x}\in[E-F]) \quad (32)$$

$$\dot{u}_{1,2}(\boldsymbol{x})=0 \text{ and } \dot{u}_2(\boldsymbol{x})=0 \quad (\boldsymbol{x}\in[F-A]) \quad (33)$$

$$p(\boldsymbol{x})=0 \quad (\boldsymbol{x}\in[E-F]), \quad (34)$$

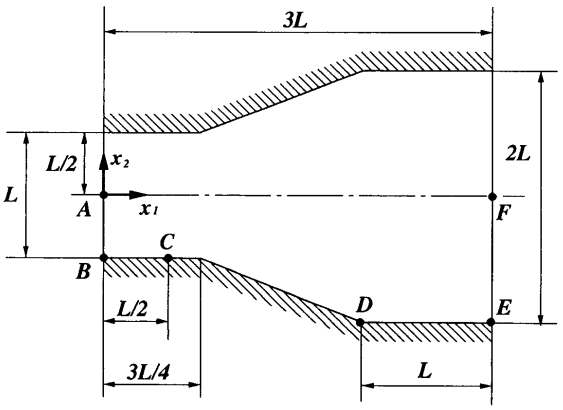

Fig. 2 Initial shape of two-dimensional symmetrically enlarged channel

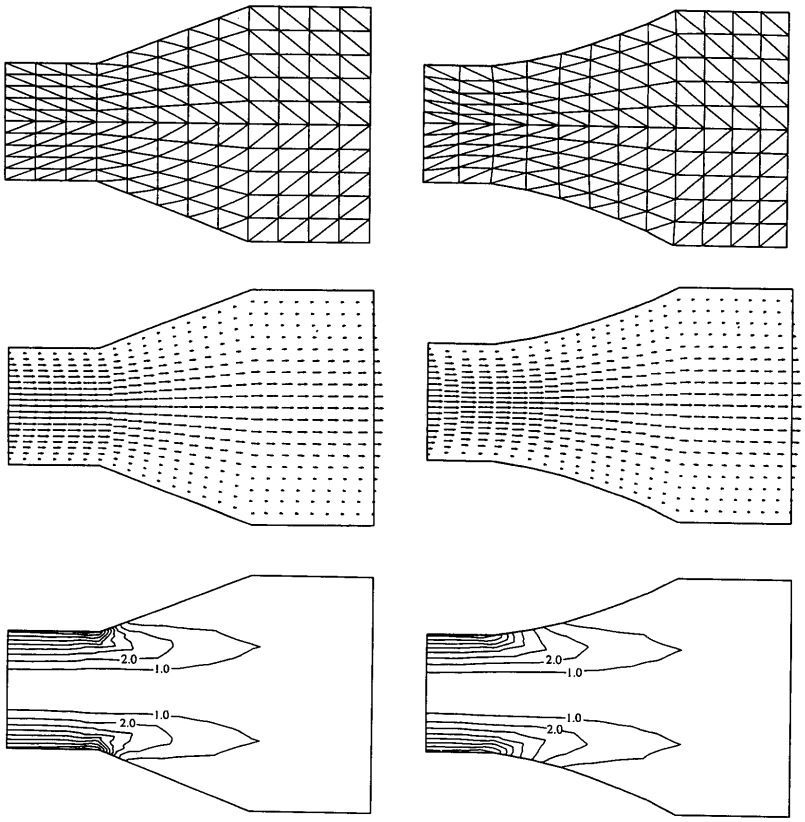

Fig. 3 Results by the growth-strain method: Comparison between finite-element meshes (upper), flow velocity maps (middle) and distributions of dissipated energy density (lower) at initial state (left) and at converged state after twenty iterations (right)

where the Reynolds number Re is defined as

$$Re=\frac{\rho\bar{u}L}{\mu}. \tag{35}$$

In the shape deformation analyses, a free boundary on [C-D], slide constraints on [B-C], [D-E] and [F-A], and a complete constraint on [A-B] and [E-F] were assumed.

The flow fluid analyses were performed using the triangular elements, the shape functions of which were of second order in velocity and first order in pressure[7]. The shape deformation analyses were carried out using triangular elements of first order in displacement. For $\bar{D}$ in Eq. (3), the volume average of $D(\boldsymbol{x})$ $(\boldsymbol{x}\in\Omega)$ was substituted. A value of 0.03 was taken for the growth rate h. For simplicity, $D_{ijkl}=\delta_{ik}\delta_{jl}$ was assumed. The distortion of the mesh due to shape deformation did not require any modification.

Numerical results to this problem are shown in Figs. 3 to 5. Figure 3 shows a comparison of the finite-element meshes, the flow velocity maps and the distribution of the dissipated energy density between at the initial state and at the converged state after twenty iterations of shape deformation. A detail of the comparison between these shapes is shown in Fig. 4. From these results, we can infer that the shape of the flow field became smoother, especially in the neighborhood of the bending point.

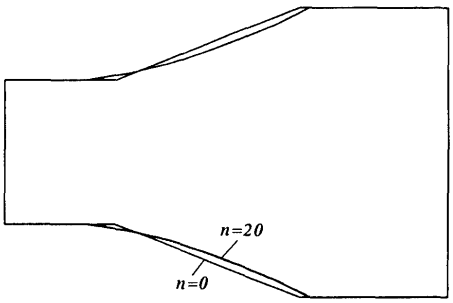

Fig. 4 Comparison of shapes at initial state and at converged state

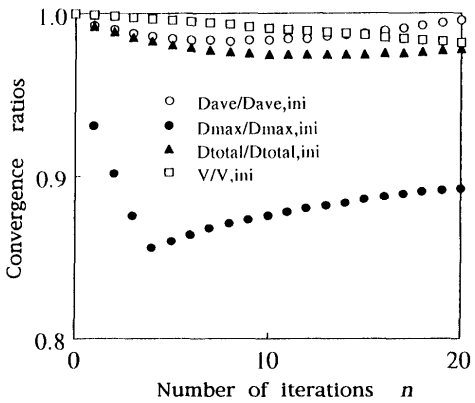

Fig. 5 Convergence ratios to initial values of maximum value D_{max} and average in volume D_{ave} of dissipated energy density, volume V and total energy dissipated D_{total}

In Fig. 5, the convergence ratios of the total energy dissipated D_{total}, the maximum value D_{max} and the average in volume D_{ave} of the dissipated energy density, and the volume V, which are normalized with the initial values, are illustrated. The bending of the path of D_{max} between iteration numbers $n=4$ and $n=5$ occurred because the location at which D_{max} exists was changed. From these results of the convergence ratios, we can conclude that the shape deformation converged at the iteration $n=20$ and that the improvements of 3% for D_{total} and 11% for D_{max} were obtained.

Based on these results, the present approach can be judged to be an effective method for minimizing the total dissipation energy.

6. Comparison with Classical Results

In this section, the results obtained by the proposed method are compared with the classical results obtained applying Gibson's suggestion[1].

The abruptly enlarged channel in Gibson's theory is dependent on the condition of the energy loss constant. With the variable height $h(x)$ and the velocity $\dot{u}(x)$ at the distance x from the end of the parallel part shown in Fig. 6, this condition is given as

$$\frac{d\dot{u}(x)^2}{dx}=\text{const.} \tag{36}$$

Employing the continuity equation, we obtain

$$\frac{1}{h(x)^2}=\frac{1}{h(0)^2}-\frac{x}{l}\left(\frac{1}{h(0)^2}-\frac{1}{h(l)^2}\right). \tag{37}$$

Figure 7 shows the result for the channel designed using Eq. (37) and analyzed by the finite-element method. The comparison between the shapes is shown in Fig. 8. The followings are the results of numerical comparison.

$$\frac{D_{max}^{(n=20)}}{D_{max}^{C}}=1.007,\quad \frac{D_{ave}^{(n=20)}}{D_{ave}^{C}}=0.983$$

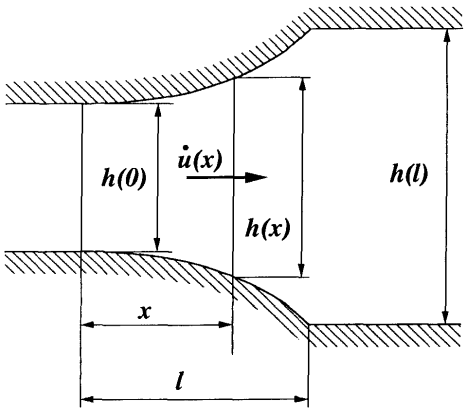

Fig. 6 Notations for enlarged channel

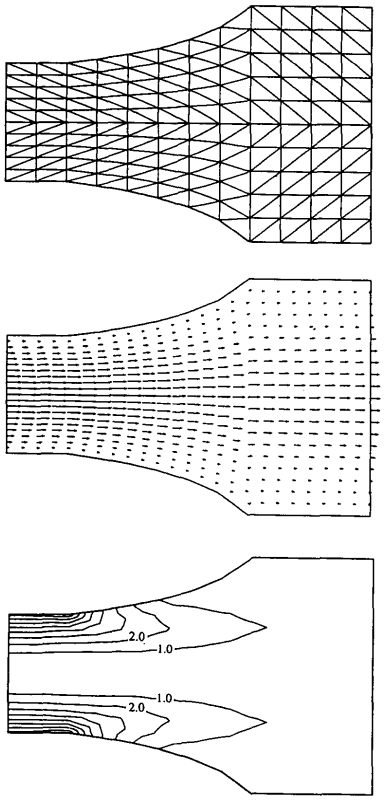

Fig. 7 Results determined under Gibson's condition: finite-element mesh (upper), flow velocity map (middle) and distribution of dissipated energy density (lower)

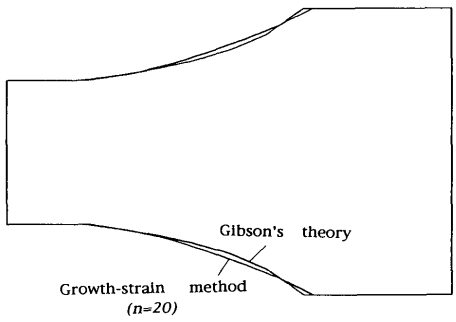

Fig. 8 Comparison between shapes obtained by the growth-strain method and those determined under Gibson's condition

$$\frac{V^{(n=20)}}{V^G}=1.007,\quad \frac{D^{(n=20)}_{\text{total}}}{D^G_{\text{total}}}=0.990$$

Here, $(\ )^{(n=20)}$ represents the results for the channel obtained by the proposed method at the iteration $n=20$ and $(\ )^G$ the results for the channel determined under the Gibson's condition.

Based on these results, it was confirmed that the shape of the channel analyzed by the proposed approach is in good agreement with the shape determined under Gibson's condition, especially in the vicinity of the beginning of enlargement.

7. Conclusions

A numerical analysis method of flow fields for minimizing the total energy dissipated was proposed. The shape deformation was achieved by the growth-strain method which consisted of analyzing the deformation of the shape by generating a bulk strain. In the flow field problems, the bulk strain was generated in proportion to the dissipated energy density. By means of the numerical examination of the two-dimensional enlarged channel problems, it was confirmed that the flow field was improved by the proposed approach. The shape of the flow field analyzed by the present approach was in good agreement with the shape determined under Gibson's condition.

Acknowledgements

This study was conducted with the support of the Saijiro Endo Memorial Fund for Scientific and Technological Promotion. The advice of Professor Kenzou Kitamura, Toyohashi University of Technology, and Professor Shoji Kinoshita, Gifu National College of Technology, was helpful in conducting the present study. We also express our grantitude to Mr. Katsuya Ohyama, graduate student of Toyohashi University of Technology, for his cooperation.

References

(1) Gibson, A. H., The Conversion of Kinetic to Pressure Energy in the Flow of Water through Passages Having Divergent Boundaries, Engineering, Feb. 16, (1912), p. 205.

(2) Azegami, H., A Proposal of a Shape-Optimization Method Using a Constitutive Equation of Growth (In the Case of a Static Body), JSME Int. J. Series I, Vol. 33, No. 1, (1990), p. 64.

(3) Azegami, H., Okitsu, A., Ogihara, T. and Takami, A., An Adaptive Growth Method for Shape Refinement, Current Topics in Structural Mechanics 1989 (ASME 1989 Pressure Vessels and Piping Conference, Honolulu, Hawaii), (1989), p. 199.

(4) Azegami, H., Ogihara, T. and Takami, A., Analysis of Uniform-Strength Shape by the Growth-Strain Method (Application to the Problems of Steady-State Vibration), JSME Int. J. Series III, Vol. 34, No. 3, (1991), p. 355.

(5) Azegami, H. and Takami, A., The Growth-Strain Method Based on the Inverse Variational Principle (An Approach to Maximum-Stiffness Shape Analysis), Trans. Jpn. Soc. Mech. Eng., (in Japanese), Vol. 56, No. 530, A(1990), p. 2162.

(6) Azegami, H., Katamine E., Imaizumi, T. and Okitsu, A., Shape-Optimization Analysis for Wire Cross-Sections of Cylindrically Coiled Spring by Growth-Strain Method, Trans. Jpn. Soc. Mech. Eng., (in Japanese), Vol. 56, No. 531, A(1990),

p. 2339.

(7) Bercovier, M. and Pironneau, O., Error Estimates for Finite Element Method Solution of the Stokes Problem in the Primitive Variables, Numer. Math., Vol. 33, (1979), p. 211.

(8) Taylor, C. and Hood, P., A Numerical Solution of the Navier-Stokes Equations usingthe Finite Element Technique, Computer and Fluids, Vol. 1, (1973), p. 73.